Supplementary Materials for

GPR84-PET imaging visualizes tumor-associated myeloid cells in brain metastases

Renesmee C. Kuo[1,2], Samantha T. Reyes[2], Rohit Verma[3], Piper Mahn[2], Sydney C. Nagy[2], Mausam Kalita[2], Bo Zhang[2], Andrew Setiadi[2], Shreya Kumar[3], Gianna Tuffley[2], Amirreza Ehsani[3], Samuel Aubert[4], Josué Ballesteros-Álvarez[4], Pedro Machado Almeida[4], Pauline Chu[5], Israt S. Alam[2], Gayatri Gowrishankar[2], Graeme Milligan[6], Hannes Vogel[5], Michael Lim[3], Melanie H. Gephart[3], Michelle L. James[2,7*]

[1]*Department of Electrical Engineering, Stanford University, Stanford, CA 94305, USA.*

[2]*Molecular Imaging Program at Stanford, Department of Radiology, Stanford University, Stanford, CA 94305, USA.*

[3]*Department of Neurosurgery, Stanford University, Stanford, CA 94305, USA.*

[4]*Lunaphore Technologies, Tolochenaz, Switzerland.*

[5]*Department of Pathology, Stanford University, Stanford, CA 94305, USA.*

[6]*Centre for Translational Pharmacology, School of Molecular Biosciences, College of Medical, Veterinary and Life Sciences, University of Glasgow, Glasgow G12 8QQ, Scotland, U.K.*

[7]*Department of Neurology and Neurological Sciences, Stanford University, Stanford, CA 94305, USA.*

*Corresponding author:

Michelle L. James, 3172 Porter Drive, Room 273, Palo Alto, CA 94304; E-mail: mljames@stanford.edu

Supplementary Figures

- **Figure S1:** [^{11}C]MGX-38 and [^{18}F]MGX-110S bind specifically to GPR84 and highly specific to GPR84 and cross the healthy, intact BBB
- **Figure S2:** GPR84 is selectively expressed on myeloid cells in human melanoma brain metastases
- **Figure S3:** Immune checkpoint blockade with anti-PD-1 and anti-CTLA-4 effectively reduces intracranial and extracranial tumor burden in a murine melanoma brain metastasis model
- **Figure S4:** GPR84 expression colocalizes with tumor-associated myeloid cells and not non-myeloid populations in a murine intracranial melanoma implant model
- **Figure S5.** Flow cytometric characterization of GPR84 expression in resident microglia and infiltrating macrophages in murine intracranial melanoma tumors
- **Figure S6.** GPR84-PET enables detection of maladaptive myeloid cells in melanoma brain metastasis mice

- **Figure S7:** Validation of anti-GPR84 antibody specificity
- **Figure S8:** GPR84 is not expressed on astrocytes and neurons in human brain metastasis

Supplementary Tables

- **Table S1:** Canonical lineage markers used to annotate Leiden clusters in Figure 1A
- **Table S2:** Marker genes used to annotate myeloid phenotypes in Figure 1C
- **Table S3:** Primary antibody details used for seqIF
- **Table S4:** Secondary antibody details used for seqIF
- **Table S5:** RNAscope Hiplex probes used for RNA detection with the RNAscope Hiplex Pro assay on COMET
- **Table S6:** PET analysis and tumor-to-background ratios in melanoma brain metastasis mice
- **Table S7:** RNA and protein panel used for RNA and protein detection on MACSima

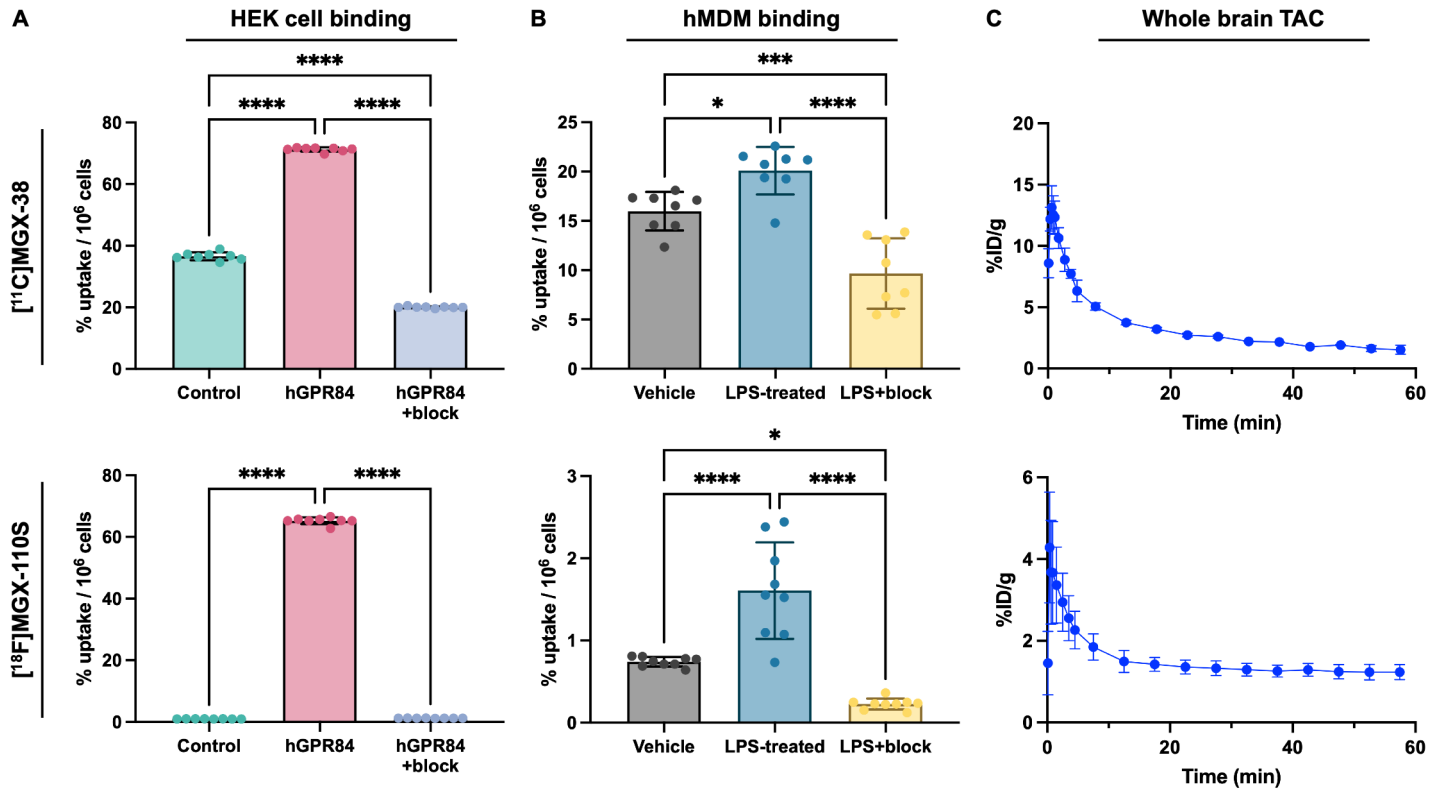


Figure S1. [^{11}C]MGX-38 and [^{18}F]MGX-110S bind specifically to GPR84 and highly specific to GPR84 and cross the healthy, intact BBB. (**A**) Both GPR84-PET tracers showed significantly increased binding to hGPR84-expressing HEK293 cells compared with parental controls, and binding was reduced by co-incubation with the GPR84 antagonist GLPG1205 (n = 8/group). (**B**) In human monocyte-derived macrophages (hMDMs), tracer binding increased markedly after LPS stimulation compared with vehicle-treated cells (n = 8/group for [^{11}C]MGX-38 and n = 9/group for [^{18}F]MGX-110S). (**C**) Whole-brain time-activity curves (TAC) from healthy C57BL/6 mice (n = 5) demonstrated rapid brain uptake of both tracers followed by good washout over the 60-min dynamic PET/CT scan. Statistical analyses were performed using one-way ANOVA with Tukey's multiple comparisons test. * denotes direct comparison of groups (*P < 0.05; ***P < 0.001; ****P < 0.0001). Data are means ± SD.

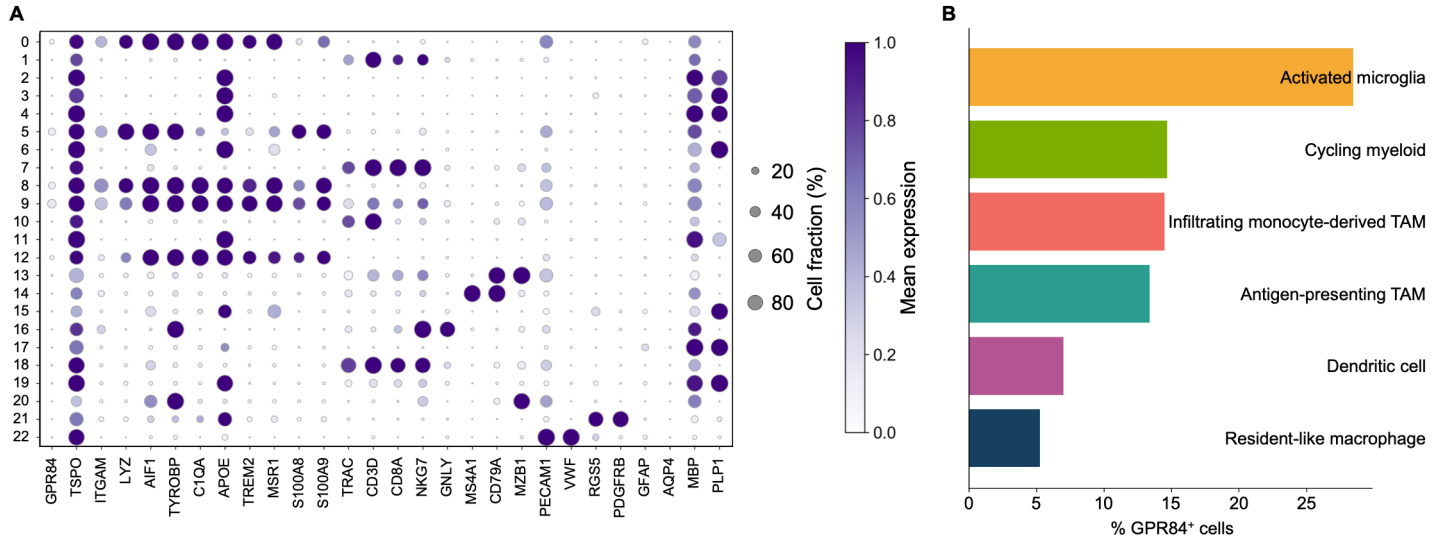


Figure S2. GPR84 is selectively expressed on myeloid cells in human melanoma brain metastases. (**A**) Dot plot showing *GPR84*, *TSPO*, and canonical lineage marker expression across Leiden clusters identified from five treatment-naïve melanoma brain metastases. Dot size represents the percentage of cells within each cluster expressing the indicated gene, and color intensity reflects mean log-normalized expression. (**B**) Proportion of GPR84^{+} cells within each annotated myeloid phenotype shown in Figure 1C-E.

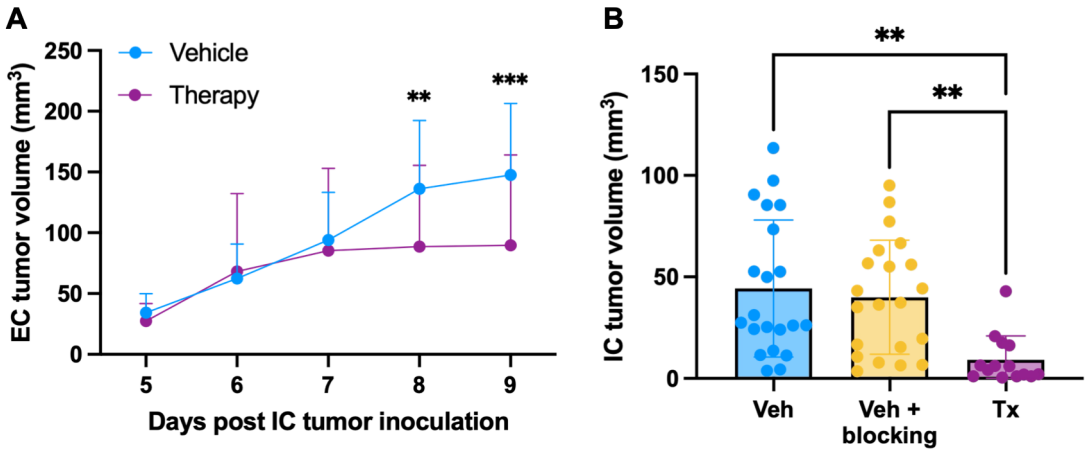


Figure S3. Immune checkpoint blockade with anti-PD-1 and anti-CTLA-4 effectively reduces intracranial and extracranial tumor burden in a murine melanoma brain metastasis model. (**A**) Extracranial tumor growth curves from days 5-9 post-intracranial tumor inoculation in vehicle- (n = 20) and ICI-treated (n = 15) groups. (**B**) T2-weighted MRI measurements of intracranial tumor volume on day 9 post-tumor implantation in vehicle-treated (n = 21), vehicle with blocking (n = 21), and therapy-treated mice (n = 14). Statistical analyses were performed using Mann-Whitney tests (A) or one-way ANOVA with Tukey's multiple comparisons test (B). * denotes direct comparison of groups (**$P < 0.01$; ***$P < 0.001$). Data are means ± SD. Veh, vehicle; Tx, therapy; IC, intracranial; EC, extracranial.

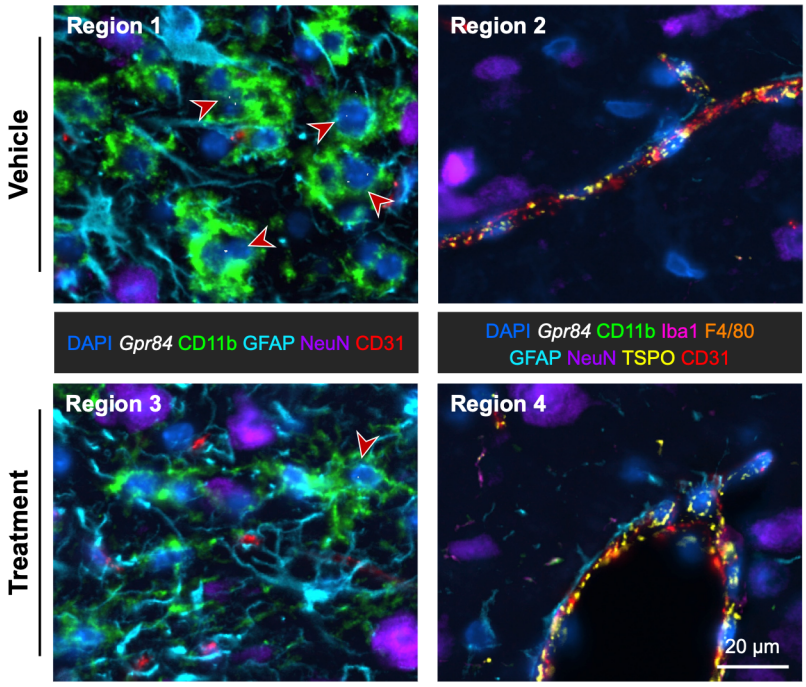


Figure S4. GPR84 expression colocalizes with tumor-associated myeloid cells and not non-myeloid populations in a murine intracranial melanoma implant model. Representative high-magnification multiplex images from the same regions shown in Figure 2B. In vehicle-treated tumor tissue (Region 1), *Gpr84* mRNA (white; red arrowheads) spatially colocalized with $CD11b^+$ myeloid cells (green), whereas little to no spatial correspondence was observed with $GFAP^+$ astrocytes (cyan), $NeuN^+$ neurons (purple), or $CD31^+$ endothelial cells (red). The contralateral healthy brain region from the same animal (Region 2) showed minimal *Gpr84* signal and no accumulation of activated myeloid cells. In therapy-treated tumor tissue (Region 3), *Gpr84* signal was markedly reduced despite the presence of more dispersed, ramified myeloid cells. The contralateral brain (Region 4) similarly showed minimal to no detectable *Gpr84* signal. TSPO (yellow) was detected along $CD31^+$ vascular structures (red). DAPI (blue) marks nuclei. Scale bar, 20 µm.

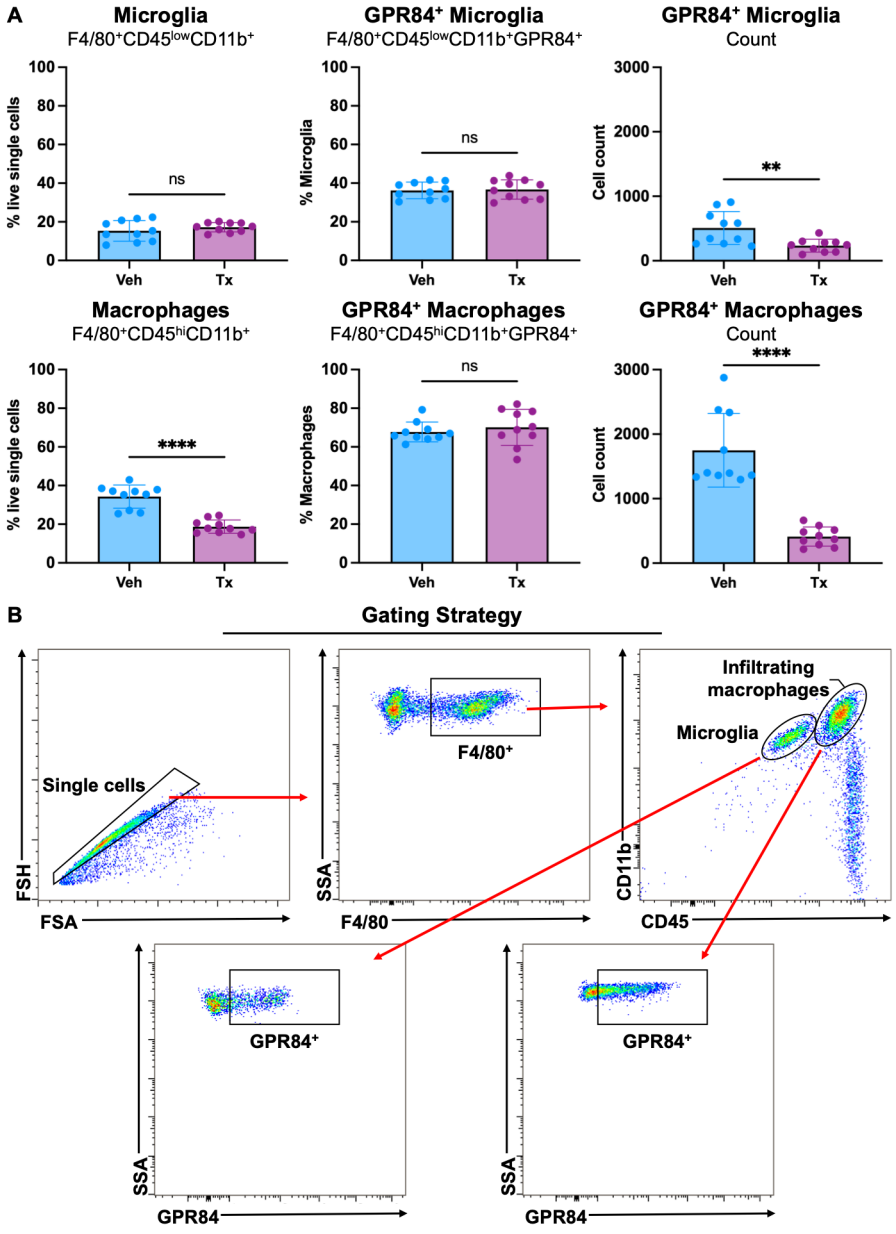


Figure S5. Flow cytometric characterization of GPR84 expression in resident microglia and infiltrating macrophages in murine intracranial melanoma tumors. (**A**) Quantification of resident microglia ($F4/80^{+}CD45^{low}CD11b^{+}$) and infiltrating macrophages ($F4/80^{+}CD45^{hi}CD11b^{+}$), expressed as a percentage of live single cells; the proportion of $GPR84^{+}$ cells within each respective myeloid population; and absolute counts of $GPR84^{+}$ microglia and $GPR84^{+}$ infiltrating macrophages in vehicle-treated and ICI-treated mice (n = 10/group). (**B**) Representative flow cytometry gating strategy. Live single cells were gated on $F4/80^{+}$ myeloid cells, followed by separation of $CD45^{low}CD11b^{+}$ microglia and $CD45^{hi}CD11b^{+}$ infiltrating macrophages. GPR84 expression was subsequently assessed within each population. Statistical analyses were performed using Mann-Whitney tests. * denotes direct comparison of groups (ns, $P > 0.05$; $^{**}P < 0.01$; $^{****}P < 0.0001$). Data are means ± SD. Veh, vehicle; Tx, therapy.

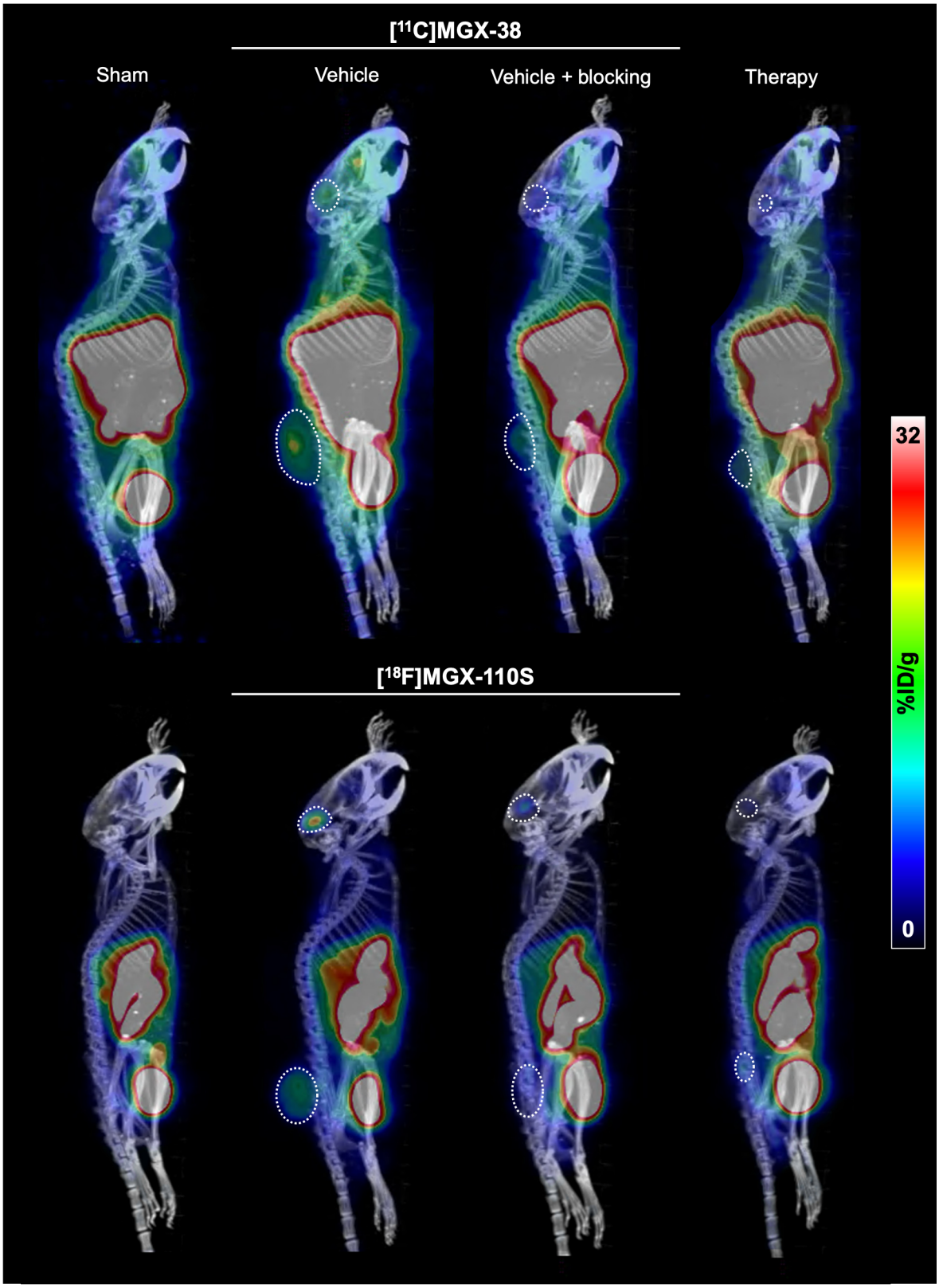


Figure S6. GPR84-PET enables detection of maladaptive myeloid cells in melanoma brain metastasis mice. Representative PET/CT whole-body MIP images highlighting elevated signal in brain and flank tumors in vehicle-treated mice compared with therapy- and vehicle-treated mice co-administered with GPR84 antagonist GLPG1205 (2 mg/kg).

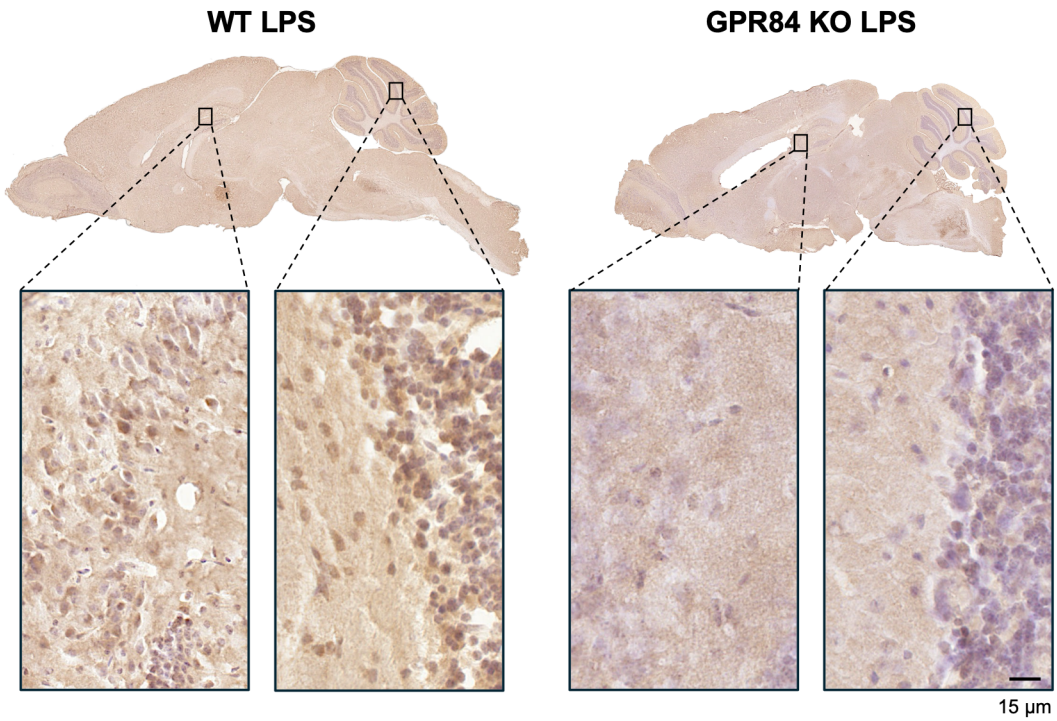


Figure S7. Validation of anti-GPR84 antibody specificity. Representative immunohistochemical staining of sagittal brain sections from systemic LPS-challenged wild-type (WT) and GPR84-knockout (GPR84 KO) mice using a polyclonal anti-GPR84 antibody. Regions with disease pathology in LPS-challenged mice (e.g., hippocampus and cerebellum) are shown at higher magnification (40x) below. Scale bar, 15 µm.

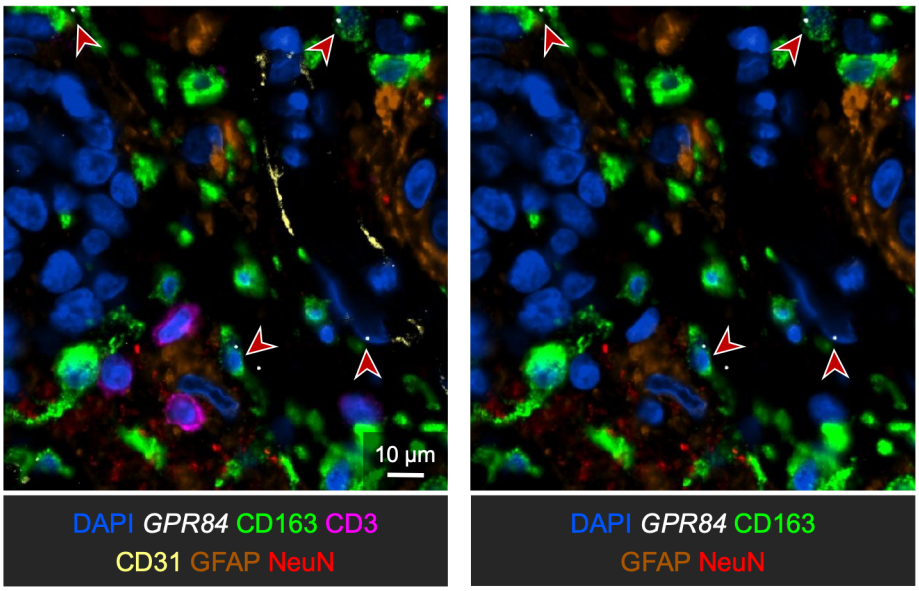


Figure S8. GPR84 is not expressed on astrocytes and neurons in human brain metastasis. Representative multiplex spatial RNA-protein images from the same FFPE tissue section shown in Fig. 6 demonstrate GPR84 RNA (white) together with CD163 (green), CD3 (magenta), CD31 (yellow), GFAP (brown), and NeuN (red) protein expression. GPR84^{+} cells are shown with red arrowheads. The right image shows the same region, omitting CD3 and CD31 to better visualize the spatial relationship among GPR84, CD163, GFAP, and NeuN. DAPI (blue) marks nuclei. Scale bar, 10 µm.

Supplementary Table 1. Canonical lineage markers used to annotate Leiden clusters in Figure 1A.

Cell type	Genes
Myeloid cell	LST1, TYROBP, FCER1G, AIF1, CTSS, LILRB1, C1QA, C1QB, C1QC, CSF1R
Malignant melanoma	MLANA, PMEL, MITF, TYR, DCT, SOX10, MIA, S100B, PRAME
T cell	CD3D, CD3E, CD3G, TRAC, TRBC1, TRBC2, IL7R, LTB
NK cell	NKG7, GNLY, KLRD1, KLRF1, PRF1, GZMB, FCGR3A
B cell	MS4A1, CD79A, CD79B, CD37, CD74, HLA-DRA, CD22, BANK1
Plasma cell	MZB1, JCHAIN, SDC1, XBP1, DERL3, IGHG1, IGKC
Fibroblast/MSC-like	COL1A1, COL1A2, COL3A1, DCN, LUM, COL6A1, COL6A2, PDGFRA
Endothelial cell	PECAM1, VWF, KDR, EMCN, RAMP2, ESAM, ENG, PLVAP
Pericyte/vSMC	RGS5, PDGFRB, CSPG4, MCAM, ACTA2, TAGLN, MYL9, NOTCH3
Oligodendrocyte	OLIG1, OLIG2, MBP, MOG, PLP1, MAG, MOBP

Supplementary Table 2. Marker genes used to annotate myeloid phenotypes in Figure 1C.

Myeloid phenotype	Genes
Resident-like macrophage	FOLR2, SELENOP, F13A1, SLC40A1, MRC1, STAB1, DAB2, MAF
Antigen-presenting TAM	HLA-DRA, HLA-DRB1, HLA-DQB1, HLA-DPA1, HLA-DPB1, CD74, APOE, GPNMB
Infiltrating monocyte-derived TAM	FCN1, S100A8, S100A9, S100A12, VCAN, LYZ, TREM1, AQP9, PLAUR, BCL2A1
Activated microglia	P2RY12, OLFML3, NAV3, SLC2A5, TREM2, C3, CCL3, CCL4, CH25H
Cycling myeloid	MKI67, TOP2A, CENPF, UBE2C, CDK1, TYMS, STMN1
Dendritic cell	CD1C, CLEC10A, CLEC9A, XCR1, IRF8, FLT3, LAMP3, CCR7, FSCN1

Supplementary Table 3. Primary antibody details used for seqIF.

Cycle	Marker	Antibody clone	Supplier	Catalog number	Dilution
1	CD31	EP3095	Abcam	AB76533	1:200
2	NeuN	EPR12763	Abcam	AB177487	1:1500
3	CD11b	EPR1344	Abcam	AB133357	1:5000
4	Iba1	EPR16588	Abcam	AN178846	1:8000
5	GFAP	Polyclonal	Abcam	AB4674	1:10000
6	F4/80	D4C8V	Cell Signaling Technology	30325S	1:450
7	TSPO	EPR[5384]	Abcam	AB109497	1:45000

Supplementary Table 4. Secondary antibody details used for seqIF.

Cycle	Raised in species	Anti-species	Supplier	Fluorophore	Catalog number	Dilution
1	Goat	Rabbit	Lunaphore	AF555	DR555RB	1:100
2	Goat	Rabbit	Lunaphore	AF555	DR555RB	1:200
3	Goat	Rabbit	Lunaphore	AF647	DR647RB	1:200
4	Goat	Rabbit	Lunaphore	AF647	DR647RB	1:200
5	Goat	Chicken	Lunaphore	AF555	A32932	1:200
6	Goat	Rabbit	Lunaphore	AF647	DR647RB	1:200
7	Goat	Rabbit	Lunaphore	AF647	DR647RB	1:200

Supplementary Table 5. RNAscope Hiplex probes used for RNA detection with the RNAscope Hiplex Pro assay on COMET.

Cycle	Marker	Channel	Supplier	Catalog number	Dilution
1	*Gfap*	FITC	ACD	313217-T1	1:50
1	*Gpr84*	TRITC	ACD	438377-T2	1:50
2	*Ppib*	TRITC	ACD	313917-T6	1:50
2	*Hprt*	Cy5	ACD	312957-T7	1:50
2	*Ubc*	Cy7	ACD	310777-T8	1:50

Supplementary Table 6. PET analysis and tumor-to-background ratios in melanoma brain metastasis mice.

		IC tumor (%ID/g)	Healthy brain (%ID/g)	Tumor-to-brain ratio	EC tumor (%ID/g)	Muscle (%ID/g)	Tumor-to-muscle ratio
[^{11}C]MGX-38	**Vehicle**	10.85 ± 1.24	6.22 ± 1.03	1.74	10.45 ± 1.63	6.00 ± 1.71	1.74
	Therapy	8.78 ± 0.69	5.71 ± 1.03	1.54	8.08 ± 1.08	6.16 ± 0.75	1.31
[^{18}F]MGX-110S	**Vehicle**	6.14 ± 1.89	1.13 ± 0.30	5.43	4.08 ± 1.02	1.91 ± 0.47	2.14
	Therapy	3.13 ± 0.91	1.15 ± 0.22	2.72	2.91 ± 0.66	1.69 ± 0.22	1.72

Supplementary Table 7. RNA and protein panel used for RNA and protein detection on MACSima.

RNA	Protein	Cycle	Marker	Clone	Supplier	Fluorophore	Catalog #	Incubation time
✓		**1**	GPR84	N/A	Miltenyi Biotec	AF647	130-137-060	15
	✓	**1**	CD3	REA1151	Miltenyi Biotec	APC	130-120-26	10
	✓	**2**	CD163	REA1309	Miltenyi Biotec	PE	130-127-908	10
	✓	**3**	CD31	REA1312	Miltenyi Biotec	PE	130-128-769	10
	✓	**4**	GFAP	REAL735	Miltenyi Biotec	PE	130-125-681	10
	✓	**5**	NeuN	REA1131	Miltenyi Biotec	PE	130-119-493	10